Nonreciprocal Surface Acoustic Waves in Multilayers with Magnetoelastic and Interfacial Dzyaloshinskii-Moriya Interactions

Roman Verba, Ivan Lisenkov, Ilya Krivorotov, Vasil Tiberkevich, and Andrei Slavin

Phys. Rev. Applied **9**, 064014 — Published 12 June 2018

DOI: 10.1103/PhysRevApplied.9.064014

Nonreciprocal surface acoustic waves in multilayers with magneto-elastic and interfacial Dzyaloshinskii-Moriya interactions

Roman Verba,[1] Ivan Lisenkov,[2,3,*] Ilya Krivorotov,[4] Vasil Tiberkevich,[5] and Andrei Slavin[5]

[1] *Institute of Magnetism, Kyiv 03680, Ukraine*
[2] *School of Electrical Engineering and Computer Science, Oregon State University, Corvallis, OR 97333, USA*
[3] *Kotelnikov Institute of Radioengineering and Electronics, Russian Academy of Sciencies, Moscow 125009, Russia*
[4] *Department of Physics and Astronomy, University of California, Irvine, California 92697, USA*
[5] *Department of Physics, Oakland University, Rochester, MI 48309, USA*

Surface acoustic waves (SAW) propagating in a piezoelectric substrate covered with a thin ferromagnetic/heavy metal bilayer are found to exhibit a substantial degree of nonreciprocity, i.e. the frequencies of these waves are non-degenerate with respect to the inversion of the SAW propagation direction. The simultaneous action of the magneto-elastic interaction in the ferromagnetic layer and the interfacial Dzyaloshinskii-Moriya interaction (IDMI) in the ferromagnetic/heavy metal interface, results in the openings of magneto-elastic bandgaps in the SAW spectrum, and the frequency position of these bandgaps are different for opposite SAW propagation directions. The bandgap widths and the frequency separation between them can be controlled by a proper selection of the magnetization angle and the thickness of the ferromagnetic layer. Using numerical simulations we demonstrate that the isolation between SAWs propagating in the opposite directions in such a system can exceed the direct SAW propagation losses by more than one order of magnitude.

I. INTRODUCTION

Surface acoustic waves (SAWs) transmission lines, based on high-quality piezoelectric single crystals, find applications as frequency filters, sensors, and other signal processing devices [1–4]. SAWs have very low propagation losses in the frequency range from megahertz to several gigahertz. They can be excited with a very high efficiency in piezoelectric crystals, and the use of unidirectional transducers [3, 4] can reduce the insertion losses of a SAW transmission lines to just several dB. Moreover, typical propagation speeds (and, therefore, wavelengths) of SAWs in crystals are several orders of magnitude less than the speed of electromagnetic waves, thus allowing the miniaturization of SAW signal processing devices, compared to their electromagnetic counterparts.

A typical frequency spectrum $\omega_{\boldsymbol{k}}$ of a SAW is reciprocal, i.e. it is degenerate for the SAWs having opposite wave vectors $\boldsymbol{k}$ and $-\boldsymbol{k}$: $\omega_{\boldsymbol{k}} = \omega_{-\boldsymbol{k}}$. This degeneracy is a result of a fundamental time-reversal symmetry in the laws of mechanics. However, frequency nonreciprocity (when $\omega_{\boldsymbol{k}} \neq \omega_{-\boldsymbol{k}}$) is extremely important for applications: it allows to isolate signals traveling in the opposite directions [5, 6]. From a practical point of view, a good isolator should demonstrate high rejection, i.e. should be blocking most of the power traveling in one direction (say, from port "2" to port "1"), and, simultaneously, low insertion loss, i.e. should be transmitting nearly all the power traveling in the opposite direction (from port "1" to port "2"). It is known that SAW-based devices demonstrate very low transmission losses, and, therefore, should be useful as isolators, if a nonreciprocal propagation SAW propagation in these devices can be demonstrated.

Unfortunately, a nonreciprocal propagation of SAW is not easy to achieve. So far, the nonreciprocal propagation of SAW was found in devices with moving or rotating elements [7, 8], where the effect of the summation of velocities of sound and moving media was used. An alternative way to achieve acoustic nonreciprocity is to use nonlinear effects in high-power acoustic waves, where the acoustic wave loss or gain are power-dependent [9–12]. Unfortunately, both these ways did not lead to the development of practical nonreciprocal devices based on acoustic waves.

In contrast to acoustic waves, the frequency nonreciprocity of spin waves (SWs) propagating in ferromagnetic media is not an exotic phenomenon. The SW nonreciprocity is a consequence of the intrinsic breaking of time-reversal symmetry in magnetized magnetic materials, where magnetization precesses only clockwise around its equilibrium direction. The frequency nonreciprocity for SWs can be achieved in multiple ways, e.g. by non-symmetric boundary conditions [13–15], by patterning of a ferromagnet [16–18], or by bulk or interfacial Dzyaloshinskii-Moriya interaction [19–22]. It should be noted, that the application of the SWs themselves for the development of compact nonreciprocal microwave devices is a challenging task, as the magnetic field bias is needed, and the problem of a relatively high SW propagation losses should be solved.

Fortunately, due to the magneto-elastic interaction in magnetostrictive materials, the SWs and acoustic waves can interact with each other, and SWs can act as a "source" of nonreciprocity for acoustic waves. The nonreciprocity of magneto-elastic waves [23–25], as well as

* ivan.lisenkov@phystech.edu

the magneto-elastic interaction itself [26–28], were studied for a long time in the case of bulk samples. The bulk materials, however, typically do not show good acoustic, magnetic, magneto-elastic and piezoelectric properties simultaneously, which hinders their practical applications in nonreciprocal devices. For example, many papers were devoted to the studies of magneto-elastic waves in yttrium-iron garnet (YIG), which has nice magnetic properties, but the magneto-elastic interaction in YIG is weak, and this material has no piezoelectricity at all. At the same time, metallic ferromagnets (such as Ni, Co, Fe) have rather large magnetostriction (3-4 order larger than in YIG), but prohibitively bad acoustic properties.

Rather promising recent experiments [29–32] have demonstrated that the propagation of SAWs in piezoelectric substrates can be controlled by a thin magnetic layer placed atop the substrate. The use of such heterostructures allows one to combine in a single device a high-quality piezoelectric substrate (like $LiNbO_3$) and a ferromagnet with large magnetostriction (e.g., Ni). Moreover, it has been shown that SAWs propagating in a $LiNbO_3$ substrate covered by a thin Ni film, indeed, demonstrate some degree of nonreciprocity [32], although the observed nonreciprocity effect was small. In such a case the SWs are generally reciprocal, and the small transmission nonreciprocity comes from the slightly different widths of the magneto-elastic bandgaps having the same central frequency in the SAW spectrum for waves with opposite wave vectors. As a result, the nonreciprocal transmission appears on a background of large propagation (insertion) losses.

In this work we propose a way to substantially enhance the nonreciprocal properties of SAW in piezoelectric/ferromagnetic heterostructures using the materials with interfacial Dzyaloshinskii-Moriya interaction (IDMI). We show, that IDMI results in a non-degeneracy of the *central frequencies* of the magneto-elastic bandgaps with respect to the inversion of the SAW propagation direction. Since the central frequencies of the bandgaps are different for the two counter-propagating waves, a wave traveling in one direction falls within the bandgap, while the wave traveling in the opposite direction does not "feel" the bandgap at all. Therefore, the damping of the wave propagating in one direction is tremendously increased, while for the wave propagating in the opposite direction is practically unaffected, resulting in the simultaneously high isolation and low insertion losses. In our numerical simulations we used the parameters of a transmission line based on a $LiNbO_3$ substrate covered by a thin Ni/Pt bilayer, and showed, that, using a high quality Ni film, one can achieve the isolation of up to 45 dB with the insertion losses of about 20 dB.

The article is organized as follows. In Sec. II we present a general formalism for the magneto-elastic coupling between the linear SWs and SAWs in the framework of a perturbation theory. Then, we consider the conditions for the appearance of nonreciprocal magneto-elastic bandgaps in the wave spectrum (Sec. III B), and the ways for the optimization of the nonreciprocal properties (Sec. III C). Finally, Sec. III D is devoted to the calculation of the SAW line transmission characteristics in the presence of IDMI and the SAW coupling to SW.

II. THEORY OF WEAKLY-COUPLED LINEAR MAGNETO-ELASTIC WAVES

In this section we revisit the theory of magneto-elastic interaction in ferromagnetic samples, and develop an analytical formalism for magneto-elastic coupling between the spin-waves and acoustic waves suitable for the systems having arbitrary wave profiles (e.g. suitable for surface magneto-elastic waves), limiting ourselves to the case of linear coupling between SWs and SAWs.

The dynamics of the magneto-elastic waves is governed by the coupled Landau-Lifshitz equation for SWs and elastic mechanical equations [2, 5] for acoustic waves. Simulations solution of these equations is complicated, and often possible only numerically [33–36]. However, in almost all the practically important situations the magnetostriction is weak in comparison to the other interactions in a ferromagnet, which allows us to consider the magneto-elastic interaction in the framework of a perturbation theory.

For the consideration of linear excitations the magnetization vector $\boldsymbol{M}$ can be represented as a sum of a static and dynamic components, $\boldsymbol{M}(\boldsymbol{r},t) = M_s\left[\boldsymbol{\mu}(\boldsymbol{r}) + \boldsymbol{m}(\boldsymbol{r},t)\right]$, where M_s is the saturation magnetization, $\boldsymbol{\mu}$ is the unit vector pointing in the direction of the static magnetization, and $\boldsymbol{m}$ is a dimensionless dynamic magnetization ($|\boldsymbol{m}| \ll 1$). Then, the equations describing the coupled magneto-elastic dynamics can be written as:

$$\frac{1}{\gamma}\hat{\boldsymbol{J}}\cdot\frac{d\boldsymbol{m}(\boldsymbol{r},t)}{dt} - \int \hat{\boldsymbol{\Omega}}\cdot\boldsymbol{m}(\boldsymbol{r}',t)d\boldsymbol{r}' = \boldsymbol{b}^{\rm me}(\boldsymbol{r},t)\,, \quad (1)$$

$$\rho\frac{\partial^2}{\partial t^2}\xi_i(\boldsymbol{r},t) - c_{ijln}\frac{\partial^2}{\partial x_j\partial x_l}\xi_n(\boldsymbol{r},t) = f_i^{\rm me}(\boldsymbol{r},t)\,. \quad (2)$$

Here $\hat{\boldsymbol{J}} = \hat{\boldsymbol{e}}\cdot\boldsymbol{\mu}$ is the operator of the angular momentum, $\hat{\boldsymbol{e}}$ is the Levi-Chivita anti-symmetric tensor, $\hat{\boldsymbol{\Omega}} = \hat{\boldsymbol{\Omega}}(\boldsymbol{r},\boldsymbol{r}')$ is the operator of magnetic interactions (see Refs. 37–39 for more details),$\boldsymbol{\xi}(\boldsymbol{r},t)$ is the elastic displacement, ρ is the density, and c_{ijlm} are the components of the elastic stiffness tensor. The magneto-elastic coupling is given by the terms in the right-hand side of the equation, where $\boldsymbol{b}^{\rm me}(\boldsymbol{r},t)$ is the effective magnetic field generated by the acoustic deformations via the inverse magnetostriction, and $\boldsymbol{f}^{\rm me}$ is the effective force generated by the magnetization dynamics and acting on the sample via the direct magnetostriction effect. In Eq. (1) we skipped another coupling term of the form $\boldsymbol{m}(\boldsymbol{\mu}\cdot\boldsymbol{b}^{\rm me})$, as it is of the second-order of smallness, and cannot result in a linear coupling between the waves. In Eq. (2) and below the repeating indices $(i,j,l,m) = (x,y,z)$ are assumed to be summed.

The magneto-elastic coupling can be obtained from the following magneto-elastic energy density:

$$W^{\rm me} = \frac{1}{M_s^2} b_{ijln} u_{ij} M_l M_n \,, \tag{3}$$

where $\hat{\boldsymbol{b}}$ is the tensor of magnetostriction [40] and $\hat{\boldsymbol{u}}(\boldsymbol{r},t)$ is the tensor defining the strain created by the displacement $\boldsymbol{\xi}(\boldsymbol{r},t)$ [2]:

$$u_{ij} = \frac{1}{2}\left(\frac{\partial \xi_i}{\partial r_j} + \frac{\partial \xi_j}{\partial r_i}\right) \,. \tag{4}$$

The values of the field $\boldsymbol{b}^{\rm me}$ and the force $\boldsymbol{f}^{\rm me}$ can be calculated using (3) as:

$$b_n^{\rm me}(\boldsymbol{r},t) = -\frac{\partial W^{\rm me}}{\partial \boldsymbol{M}} \approx -\frac{2}{M_s} b_{ijln} u_{ij}(\boldsymbol{r},t)\mu_l(\boldsymbol{r}) \,, \tag{5}$$

$$f_i^{\rm me}(\boldsymbol{r},t) = \frac{\partial}{\partial x_i}\frac{\partial}{\partial u_{ij}} W^{\rm me} \approx 2\frac{\partial}{\partial x_j} b_{ijln}\mu_l(\boldsymbol{r}) m_n(\boldsymbol{r},t) \,, \tag{6}$$

where we left only the terms that are linear in the dynamic magnetization $\boldsymbol{m}$ or displacement $\boldsymbol{\xi}$ as they are responsible for the linear coupling between the waves. The other terms, corresponding, e.g., for the parametric coupling between the waves, are disregarded.

Eqs. (1, 2) can be solved within a standard framework of an eigenmodes expansion:

$$\boldsymbol{m}(\boldsymbol{r},t) = \sum_\nu c_\nu(t)\boldsymbol{m}_\nu(\boldsymbol{r}) + \text{c.c.} \,, \tag{7}$$

$$\boldsymbol{\xi}(\boldsymbol{r},t) = \sum_\lambda q_\lambda(t)\boldsymbol{\xi}_\lambda(\boldsymbol{r}) + \text{c.c.} \,, \tag{8}$$

where $\boldsymbol{m}_\nu(\boldsymbol{r})$ and $\boldsymbol{\xi}_\lambda(\boldsymbol{r})$ are the profiles of the linear SWs and acoustic modes, while $c_\nu(t)$ and $q_\lambda(t)$ are the unknown complex amplitudes of the eigenmodes. The spatial profiles of the eigenmodes and their eigenfrequencies, ω_ν and $\tilde{\omega}_\lambda$, respectively, are the solutions of Eqs. (1) and (2) with zero right-hand-side parts in the form $\boldsymbol{m}(\boldsymbol{r},t) = \boldsymbol{m}_\nu(\boldsymbol{r})e^{-i\omega_\nu t}$, while $\boldsymbol{\xi}(\boldsymbol{r},t) = \boldsymbol{\xi}_\lambda(\boldsymbol{r})e^{-i\tilde{\omega}_\lambda t}$.

The linear SW modes satisfy the following orthogonality relation [37, 38]:

$$\frac{M_s}{\gamma}\int \boldsymbol{m}^*_{\nu'}(\boldsymbol{r})\cdot\boldsymbol{\mu}(\boldsymbol{r})\times\boldsymbol{m}_\nu(\boldsymbol{r})d\boldsymbol{r} = -iA_\nu\delta_{\nu,\nu'} \,, \tag{9}$$

where $A_\nu > 0$ is the spin-wave normalization constant having the dimensionality of action [41]. A similar orthogonality condition can be written for the acoustic modes [2, 42]:

$$2\omega_\lambda \int \rho(\boldsymbol{r})\boldsymbol{\xi}^*_\lambda(\boldsymbol{r})\cdot\boldsymbol{\xi}_{\lambda'}(\boldsymbol{r})d\boldsymbol{r} = Q_\lambda\delta_{\lambda\lambda'} \,, \tag{10}$$

where $Q_\lambda > 0$ is a positive normalization constant having the same dimensionality as A_ν.

Substituting the expansions Eqs. (7, 8) for $\boldsymbol{m}(\boldsymbol{r},t)$ and $\boldsymbol{\xi}(\boldsymbol{r},t)$ in Eqs. (1, 2) and using the orthogonality relations, we get the following final equations for the amplitudes of the coupled spin and acoustic waves:

$$\begin{aligned} &\frac{dc_\nu}{dt} + i\omega_\nu c_\nu + \Gamma_\nu c_\nu = i\sum_\lambda \sqrt{\frac{Q_\lambda}{A_\nu}}\kappa_{\nu,\lambda} q_\lambda \,, \\ &\frac{dq_\lambda}{dt} + i\tilde{\omega}_\lambda q_\lambda + \tilde{\Gamma}_\lambda q_\lambda = i\sum_\nu \sqrt{\frac{A_\nu}{Q_\lambda}}\kappa^*_{\nu,\lambda} c_\nu \,, \end{aligned} \tag{11}$$

where we also introduce in a common way [8, 38] the damping rates of the spin and acoustic modes Γ_ν and $\tilde{\Gamma}_\lambda$, respectively. The coupling coefficient is equal to

$$\kappa_{\nu,\lambda} = \frac{2}{\sqrt{A_\nu Q_\lambda}}\int \boldsymbol{\mu}(\boldsymbol{r})\cdot\left(\hat{\boldsymbol{b}}\cdot\hat{\boldsymbol{u}}_\lambda(\boldsymbol{r})\right)\cdot\boldsymbol{m}^*_\nu(\boldsymbol{r})d\boldsymbol{r} \,. \tag{12}$$

This expression is the central result of the above developed theory. The coupling coefficient can be calculated for the arbitrary spatial profiles of the acoustic and SW modes. The exact profiles of the SW and acoustic modes, as well as the mode eigenfrequencies ω_ν and $\tilde{\omega}_\lambda$, in simple cases can be found analytically, or, otherwise, can be extracted from numeric simulations.

In the case of propagating waves, characterized by a wave vector $\boldsymbol{k}$, the solution of Eq. (11) can be easily obtained. In the equations above we change $\boldsymbol{m}_\nu \to \boldsymbol{m}_{\boldsymbol{k}}(\boldsymbol{\rho})e^{i\boldsymbol{k}\cdot\boldsymbol{r}}$ and $\boldsymbol{\xi}_\lambda \to \boldsymbol{\xi}_{\boldsymbol{k}'}(\boldsymbol{\rho})e^{i\boldsymbol{k}'\cdot\boldsymbol{r}}$, where $\boldsymbol{\rho}$ is two-dimensional radius vector, perpendicular to the wave propagation direction, defined by $\boldsymbol{k}$. Then, Eq. (12) is transformed to

$$\kappa_{\boldsymbol{k},\boldsymbol{k}'} = \frac{2}{\sqrt{A_{\boldsymbol{k}}Q_{\boldsymbol{k}'}}}\int \boldsymbol{\mu}(\boldsymbol{r})\cdot\left(\hat{\boldsymbol{b}}\cdot\hat{\boldsymbol{u}}_{\boldsymbol{k}'}(\boldsymbol{\rho})\right)\cdot\boldsymbol{m}^*_{\boldsymbol{k}}(\boldsymbol{\rho})e^{i(\boldsymbol{k}'-\boldsymbol{k})\cdot\boldsymbol{r}}d\boldsymbol{r} \,. \tag{13}$$

It is clear, that in the case when the static magnetization is uniform along the wave propagation direction, the exponent under the integral gives zero integration result until $\boldsymbol{k} \neq \boldsymbol{k}'$. Therefore, in this case the spin and acoustic waves can interact only if they have the same wave vector $\boldsymbol{k}$. Note, that the length L of the sample in the wave propagation direction, which appears after the integration in Eq. (13), is canceled by the same term in the normalization constants of SW and SAW. The dispersion relation for the interacting waves can be written as:

$$\omega_k = \frac{\omega_{\rm SW}+\omega_{\rm AW}}{2} \pm \sqrt{\left(\frac{\omega_{\rm SW}-\omega_{\rm AW}}{2}\right)^2 + |\kappa_k|^2} \,, \tag{14}$$

where $\omega_{\rm SW} = \omega_{{\rm SW},\boldsymbol{k}}$ and $\omega_{\rm AW} = \omega_{{\rm AW},\boldsymbol{k}}$ are the dispersion relations of non-interacting SWs and acoustic waves, respectively.

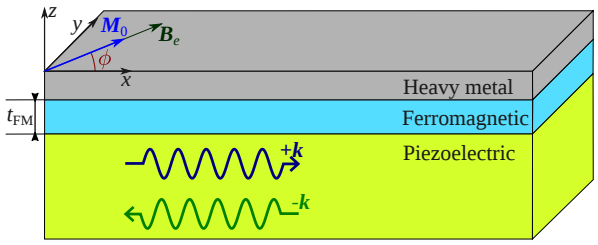

FIG. 1. A layout of the heterostructure under study – piezoelectric substrate covered by ferromagnetic/heavy metal bilayer.

III. NONRECIPROCAL SURFACE MAGNETO-ELASTIC WAVES

A. Spin-wave modes in a ferromagnetic film with IDMI

In this section we apply the above presented general theory to the study of the surface magneto-elastic waves in a magnetic/nonmagnetic heterostructure. A sketch of a considered heterostructure is shown in Fig. 1. It consists of a nonmagnetic substrate which supports propagation of a surface acoustic wave (SAW). Typically, this substrate is a piezoelectric single-crystal, like $LiNbO_3$, $LiTaO_3$ or quartz. The piezoelectric substrate is covered with a thin ferromagnetic film having a large magnetostriction (e.g. Ni), and, then, by a thin heavy metal layer (typically Pt), which induces IDMI at the ferromagnetic/heavy metal interface. The ferromagnetic layer is biased by an external magnetic field $\boldsymbol{B}_e$ applied in the film plane at the angle ϕ respective to the wave propagation direction. The value of the bias field should be sufficient to magnetize the ferromagnetic film in its plane, thus overcoming the effect of the surface perpendicular magnetic anisotropy, which can exists at the ferromagnetic / heavy metal interface.

Since IDMI is an interface effect, the thickness of a ferromagnetic film necessary to produce a significant SW nonreciprocity should be sufficiently small. As it became clear from the results of our numerical simulations, the ferromagnetic film thickness should not exceed several tens of nanometers. In this case we can use the assumption of a uniform SW profile across the thickness of a ferromagnetic layer, $\boldsymbol{m_k} \notin f(z)$. The dispersion of SWs, propagating along the x-axis (see Fig. 1), can be expressed as [20, 43]:

$$\omega_{\mathrm{SW},k} = \sqrt{\Omega_{zz}\Omega_{\mathrm{IP}}} - \omega_M \tilde{D} k \sin\phi\,, \tag{15}$$

where

$$\begin{aligned} \Omega_{\mathrm{IP}} &= \left[\omega_H + \omega_M\left(\lambda_{ex}^2 k^2 + f(kt)\sin^2\phi\right)\right]\,, \\ \Omega_{zz} &= \left[\omega_H - \omega_{an} + \omega_M\left(\lambda_{ex}^2 k^2 + 1 - f(kt)\right)\right]\,. \end{aligned} \tag{16}$$

In these equations $\omega_H = \gamma B_e$, $\omega_M = \gamma\mu_0 M_s$, $\omega_{an} = 2\gamma K_s/(M_s t_{\mathrm{FM}})$ where K_s is the constant of the surface perpendicular anisotropy, $k = k_x$, $f(x) = 1 - (1 - e^{-|x|})/|x|$ is a function describing the dynamic demagnetization, and the effect of IDMI is described by the expression $\tilde{D} = 2Db/(\mu_0 M_s^2 t_{\mathrm{FM}})$, where D is the IDMI constant, b is the thickness of an atomic monolayer of the ferromagnet [21, 44]. From Eq. (15) it is clear, that the SW dispersion is nonreciprocal, $\omega_{\mathrm{SW},k} \neq \omega_{\mathrm{SW},-k}$ if $\phi \neq 0, \pi$. Due to the symmetry of the effective field, produced by IDMI, the vector structure of the SW mode does not depend on IDMI [43], and can be expressed as $\boldsymbol{m}_k = [-m_{\mathrm{IP}}\sin\phi, m_{\mathrm{IP}}\cos\phi, im_z]$, where m_{IP} is the in-plane dynamic component of magnetization, and the relation between the magnetization dynamic components is $m_z/m_{\mathrm{IP}} = \sqrt{\Omega_{\mathrm{IP}}/\Omega_{zz}}$.

B. Analysis of the coupling of surface acoustic waves with spin waves

The calculation of a dispersion relation and mode profile of SAWs in a layered structure consisting of a piezoelectric substrate and a metallic layer is, itself, not a simple task. Thus, to simplify our analytical analysis we used several approximations. First, we considered the substrate as isotropic and non-piezoelectric, and used the Poisson ratio as an adjustable parameter, as it is often done in analytical calculations [1]. Within this approximation it is not possible to answer the question on the SAW stability, but it is possible to adequately describe the profile of the SAW mode and, therefore, to evaluate the main characteristics of the magneto-elastic coupling of SAWs and SWs.

Second, we neglected the influence of the thin metallic layer on the SAW properties. In general, shear acoustic waves in sputtered metals are slower, than the shear acoustic waves in piezoelectric single crystals. Thus, in such a system the substrate is loaded by the metal layer, and the surface acoustic wave does not have any cut-off wavenumbers [2, 45, 46]. In reality, the thickness of the ferromagnetic layer is of the order of $t_{\mathrm{Ni}} \approx 10$ nm, and the layer of the heavy metal can be as thin as 2-3 nm, because the further increase of the heavy metal thickness does not affect the strength of IDMI [47]. The SAW wavenumber for the considered range of frequencies (1-5 GHz) is of the order of $k_x < 10\mu\mathrm{m}^{-1}$. Thus, we can work in an approximation that $k_x(t_{Ni} + t_{Pt}) \ll 1$, and assume that the SAW is only weakly affected mechanically by the bilayer. Therefore, we can use the wave dispersion and the wave mode profiles calculated for a free substrate [2, 45]. It should be noted, that the above presented formalism (Sec. II) remains to be valid if one considers the exact values of both the acoustic field distribution and the SAW dispersion. This property could be useful in the future more accurate calculations of the coupling parameter κ.

Taking into account the above described approximations, we considered a Rayleigh surface acoustic wave [48]. The in-plane component of the displacement, perpendicular to SAW propagation direction, is absent, $\xi_y =$

0, so the strain tensor components $u_{xy} = u_{yz} = u_{yy} = 0$. The oscillations in the x and z directions are shifted in phase by $\pi/2$, resulting in the effective rotation in the medium over an elliptic trajectory.

The only non-zero components of the SAW strain tensor are u_{xx}, u_{zz} and u_{xz}. At the surface ($z = 0$ in Fig. 1) the off-diagonal strain component vanishes, $u_{xz}(z = 0) = 0$, while the components u_{xx} and u_{zz} remain nonzero. The dispersion of the SAW is linear, $\omega_{\mathrm{SAW},k} = c_{\mathrm{SAW}}|k|$, where c_{SAW} is the SAW velocity.

The magneto-elastic coupling tensor $\hat{\boldsymbol{b}}$ in the case of a cubic crystal (Ni, Fe, Co) has only two independent components [5]: $b_{iiii} = b_1$ and $b_{ijij} = b_2$ (for $i \neq j$), while all the other components are zero (in the case of an isotropic media $b_1 = b_2$). Noting the symmetry of the magneto-elastic tensor, we calculated the coupling coefficient κ_k for SW in the ferromagnet and a Rayleigh SAW using Eq. (12):

$$\kappa_k = \frac{2t_{\mathrm{FM}}}{\sqrt{A_k Q_k}} \left[-b_1 \bar{u}_{xx,k} m^*_{\mathrm{IP},k} \sin\phi + b_2 \bar{u}_{xz,k} m^*_{z,k}\right] \cos\phi\,, \tag{17}$$

where $\bar{u}_{ij}$ are the strain components, averaged over the ferromagnetic film thickness, and in the definition of the normalization constants A_k, Q_k (Eqs. (9, 10)) the integration over the volume is replaced by the integration over the z coordinate.

It is clear from Eq. (17), that the magneto-elastic interaction between the SW and SAW vanishes for $\phi = \pi/2$, while this angle corresponds to the maximum IDMI-induced SW nonreciprocity, see Eq. (15). As it was pointed out earlier, at the free surface the strain component $u_{xz} = 0$, so the averaged value $|\bar{u}_{xz}| \ll |\bar{u}_{xx}|$, and the coupling coefficient is mainly determined by the first term in the brackets in Eq. (17). Therefore, the coupling coefficient is approximately proportional to the function $\kappa_k \sim \sin 2\phi$, which reaches its maximum at $\phi = \pi/4$. Consequently, the maximal coupling of SW and SAW is realized for the magnetization angle close to $\phi = \pi/4$. This feature has been already observed in Refs. 29 and 32.

We also note, that the SW eigenmode does not change with the reversal of the propagation direction $\boldsymbol{m} = \boldsymbol{m}_{-k}$. At the same time, the SAW strain tensor transforms as $u_{xx,-k} = -u_{xx,k}$, $u_{xz,-k} = u_{xz,k}$ [48]. Therefore, the coupling between the SW and SAW is nonreciprocal even without IDMI, $\kappa_k \neq \kappa_{-k}$ (if $\phi \neq 0, \pi/2$), and this nonreciprocity becomes more pronounced for thicker ferromagnetic film due to an increase of $\bar{u}_{xz}$ component. Unequal coupling results in different propagation losses of SAW in opposite directions, that was observed in Ref. 32. However, to achieve a good isolation, while maintaining a low insertion loss, one should have $|\kappa_k| \ll |\kappa_{-k}|$. A simple analysis from Eq. (17) reveals, that this requirement leads to the requirement on the stain distribution $\bar{u}_{xx} \approx \bar{u}_{xz}$, that can be realized if ferromagnetic film thickness becomes of the order of the SAW penetration depth. For metallic layers this requirement is difficult to fulfill, because a thick ferromagnetic layer significantly affect the mechanical properties of the substrate, and increases the acoustic loss. However, this regime may, possibly, be implemented in dielectric single-crystal ferromagnets, such as YIG.

C. Wave spectrum and magneto-elastic bandgaps

For our numerical example demonstrating nonreciprocal surface magneto-elastic waves we have chosen a $LiNbO_3$/Ni/Pt heterostructure. $LiNbO_3$/Ni heterostructures have been already fabricated and studied in Refs. 29 and 32, and have demonstrated good magneto-elastic coupling. $LiNbO_3$ is one of the best piezoelectric materials supporting SAW propagation in the frequency range of up to 10 GHz [49], while Ni shows large magnetostriction, and the combination Ni/Pt gives the largest IDMI among the studied combinations of Ni with other heavy metals. We used the Y-cut of $LiNbO_3$ having the density $\rho = 4650\,\mathrm{kg/m^3}$ as a substrate, and the SAW was propagating along the Z-axis. The substrate had the following material parameters: longitudinal and transversal sound velocities $c_l = 7350\,\mathrm{m/s}$ and $c_t = 3600\,\mathrm{m/s}$ [50], and the corresponding SAW velocity was $c_{\mathrm{SAW}} = 3361\,\mathrm{m/s}$. For the Ni layer we used the following parameters: saturation magnetization $\mu_0 M_s = 0.66\,\mathrm{T}$, exchange stiffness $A = 9.5 \times 10^{-12}\,\mathrm{J/m^3}$ ($\lambda_{ex} = 7.4\,\mathrm{nm}$), surface perpendicular anisotropy energy $K_s = 6 \times 10^{-4}\,\mathrm{J/m^2}$, g-factor $g = 2.21$, magneto-elastic coupling coefficients $b_1 = 9.38\,\mathrm{MJ/m^3}$, $b_2 = 10\,\mathrm{MJ/m^3}$ [51, 52]. The IDMI energy at the Pt/Ni interface was equal to $D = -2.7 \times 10^{-3}\,\mathrm{J/m^2}$, the lattice constant was $b = 0.352\,\mathrm{nm}$ [53].

An example of the spectra of SW and SAW in the heterostructure is shown in Fig. 2. By selection of the magnitude of B_e and the angle ϕ of the bias magnetic field it is possible to achieve a crossing between the spectra of non-interacting SW and SAW in a desirable frequency range. The interaction between the SAW and SW leads to the opening of bandgaps in the spectrum of a magneto-elastic surface wave. The widths of the bandgaps are determined by the coupling coefficient κ_k: $\Delta\omega = 2\pi\Delta f = 2|\kappa_k|$. Since the SW spectrum is nonreciprocal, the crossing of the SW dispersion curves with the SAW spectrum takes place at different points, and the magneto-elastic bandgaps open at *different frequencies and wave-numbers* for the waves propagating in opposite directions. This feature is clearly visible in Fig. 2(b), where the central frequencies of the bandgaps are shifted by 170 MHz with respect to each other. Therefore, within the frequency range of one of the bandgaps, the SAW propagating in one direction is strongly coupled to SW forming a slow and dissipative magneto-elastic wave, while the wave traveling in the in opposite direction is almost unaffected by the magneto-elastic interaction. This property exists only due to the SW frequency nonreciprocity induced by the IDMI in our case.

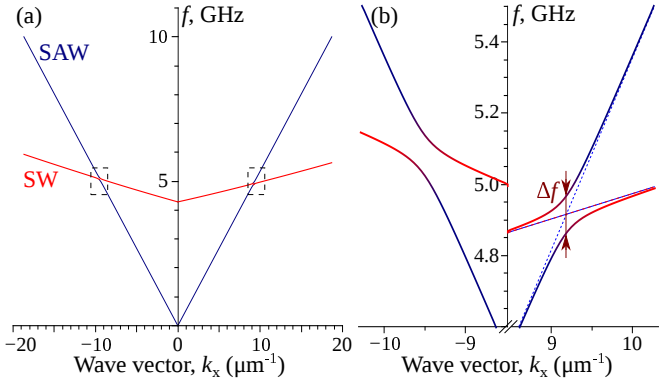

FIG. 2. (a) - Spectra of surface magneto-elastic waves in the $LiNbO_3$/Ni/Pt heterostructure, that away form the points of wave hybridization look like independent crossing spectra of SAW and SW, respectively, (b) - close view of the spectra near the hybridization points (marked by dashed rectangles in (a)), where the magneto-elastic bandgaps are clearly seen. Ni thickness $t_{\rm Ni} = 10\,$nm, magnetization angle $\phi = \pi/4$, bias field $B_e = 41\,$mT.

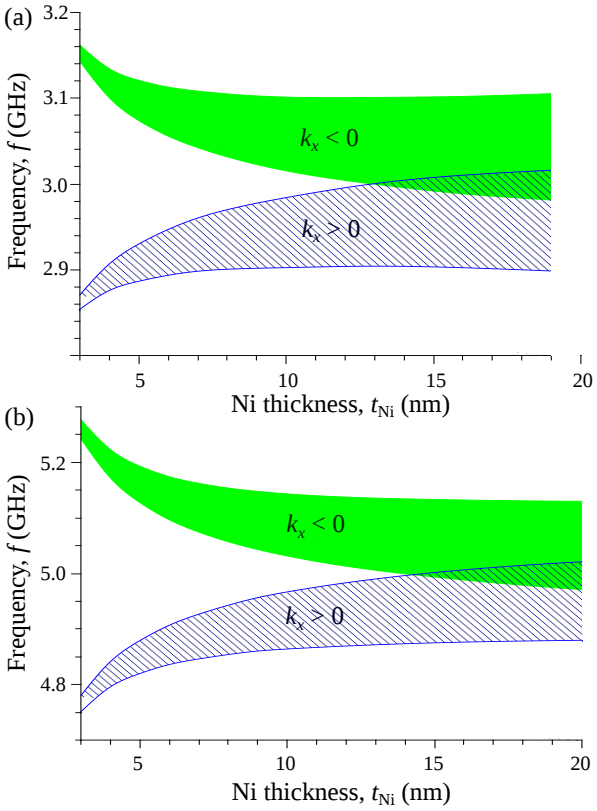

FIG. 3. Positions and widths of the magneto-elastic bandgaps in a spectrum of surface magneto-elastic waves for opposite propagation directions: (a) – for averaged frequency of 3 GHz; (b) for averaged frequency of 5 GHz. The magnetization angle is optimum, $\phi = \pi/4$.

The widths of the bandgaps and separation between their central frequencies depend on the thickness of the ferromagnetic layer. The width Δf of a bandgap increases with the thickness of the Ni layer $t_{\rm Ni}$, because the coupling coefficient between SW and SAW is proportional to $t_{\rm Ni}$, see Eq. (17). However, due to interfacial nature of the IDMI, the nonreciprocity of the SWs, and, therefore, the frequency separation between the bandgaps corresponding to the opposite propagation directions, decreases with the increase of the Ni thickness. These tendencies are clearly illustrated by Fig. 3, where the positions and the widths of the bandgaps are plotted as functions of $t_{\rm Ni}$. The bias field at each value of $t_{\rm Ni}$ was chosen in such a way, that the averaged frequency position of the bandgaps is kept constant (3 GHz in Fig. 3(a), and 5 GHz in Fig. 3(b), respectively). For applications it is desirable to have the widest possible bandgaps which, however, should be well-separated from one another, at least by a frequency interval of the order of bandgap width. Thus, there is an optimum range of the ferromagnetic film thicknesses, in which it is possible to achieve the best nonreciprocal properties of the magneto-elastic surface waves propagating in the opposite directions. For example, in the above described heterostructure $LiNbO_3$/Ni/Pt the optimum thickness of the Ni layer is $t_{\rm Ni} \approx 8 - 9\,$nm for both averaged frequencies of 3 GHz and 5 GHz (see Fig. 2). For higher averaged frequencies, the optimum Ni thickness remains almost the same, at least up to the frequency of 10 GHz, at which the SAW excitation and propagation in $LiNbO_3$ were observed experimentally in [49].

It should be noted, that the crossing and hybridization of the dispersion curves of SW and SAW at any desirable frequency cannot be always satisfied for the optimum magnetization angle of $\phi = \pi/4$. For example, for $t_{\rm Ni} > 19\,$nm the crossing cannot be achieved at the frequency below 3 GHz for any value of the bias field. This property is related to the increase of the SW group velocity at $k \to 0$ taking place with the increase of the film thickness. A solution of this problem is to use a smaller magnetization angle $\phi < \pi/4$ which decreases the SW group velocity, and even changes its sign for $\sin^2\phi < \omega_H/(\omega_H + \omega_M - \omega_{an})$. At such magnetization angles one can achieve the formation of magneto-elastic bandgaps at almost any desirable frequency. However, the widths of the bandgaps, as well as the separations between them, become smaller (see Eqs. (15, 17)). This feature limits the applicability of the IDMI-induced nonreciprocity of surface magneto-elastic waves in a relatively low-frequency range (below 2 GHz).

D. Transmission characteristics

In this section we consider how the appearance of the magneto-elastic bandgaps affects the transmission characteristics of a SAW line. In general, the appearance of the bandgaps leads to the variation of the wave group velocity $v_{gr} = \partial\omega_k/\partial k$ (slope of the dispersion curve), and to the variation of the wave damping rate in the vicinity

of the bandgaps. Both these factors contribute to the variation of a transmission rate in a magneto-acoustic transmission line.

It should be noted, that common methods of the SAW transmission calculations (see, e.g. [1, 54]) are not applicable in our case. These methods use the assumption of a negligibly small resonance linewidth, so that the wave group velocity and the efficiency of inter-digital transducers (IDTs) can be calculated locally, at the point $k = k(\omega)$. This assumption is natural for SAWs, which, typically, have a very small linewidth (for example, for $LiNbO_3$ this linewidth is only 500 kHz at the 5 GHz frequency [55]). However, the SW damping rate and, consequently, the damping rate of magneto-elastic waves in the vicinity of the bandgaps, can be comparable to (or larger than) the bandgap width. In such a case, the nonresonant wave excitation becomes important, and one should integrate contributions from all the excited waves within the resonance line.

To calculate the transmission characteristics, we need to introduce into Eq. (11) an external harmonic force, which describes the excitation of SAWs by an IDT. The application to an IDT of a microwave voltage $V(t) = V_{\rm in}e^{-i\omega t}$ of the frequency ω results in the appearance of an mechanical force in the $LiNbO_3$ substrate, and this force has a certain spatial profile, which depends on the IDT geometry. The efficiency of the coupling of IDT to a SAW, having a certain wave vector $\boldsymbol{k} = k\boldsymbol{e}_x$, can be decomposed into 2 terms.

The first of these terms is the normalized Fourier-transform F_k of the force spatial profile in the x-direction, which determines the k-dependence of the excitation efficiency. This term is often approximated by a function $F_k = \mathrm{sinc}[\pi N_f(k - k_0)/k]$, where N_f is the number of fingers in the IDT, and $\omega_0 = c_{\rm SAW}k_0$ is the central frequency of the IDT [54].

The second term describes all the other effects: piezoelectric coupling, overlap of the mechanical force with SAWs (in the z-direction), etc.. A detailed consideration of this second term lies beyond the scope of this article, and below the influence of this second term is described by a coefficient C_1. The coefficient C_1 can also be k-dependent, but this dependence is much weaker than that of the term F_k, and, therefore, is neglected below. Thus, the excitation force, which appears in the right-hand-side part of the equation for the SAW amplitudes q_k in the system Eq. (11) is expressed as $f_e(t) = C_1V_{\rm in}F_ke^{-i\omega t}$. The solution of Eq. (11) with the excitation term gives the amplitudes of the excited SAWs q_k in the form:

$$q_k = -iC_1V_{\rm in}F_k\frac{\omega - (\omega_{\rm SW} - i\Gamma_{\rm SW})}{(\omega - \omega_1)(\omega - \omega_2)}\,, \qquad (18)$$

where

$$\omega_{1,2} = \frac{\omega_{\rm SW} - i\Gamma_{\rm SW} + \omega_{\rm SAW} - i\Gamma_{\rm SAW}}{2} \pm\sqrt{\left[\frac{(\omega_{\rm SW} - i\Gamma_{\rm SW}) - (\omega_{\rm SAW} - i\Gamma_{\rm SAW})}{2}\right]^2 + |\kappa_k|^2}\,, \qquad (19)$$

and the obtained frequencies of the coupled waves are complex, because damping has been taken into account.

At the receiving IDT the displacement created by a SAW $\boldsymbol{\xi}(x) = (1/2\pi)\int \boldsymbol{\xi}_k q_k e^{ikx}dk$ is transformed into the output voltage via piezoelectric effect. Similarly to the excitation efficiency, the efficiency of detection of a SAW, having the wave vector $\boldsymbol{k}$, can be decomposed into 2 terms, and, then,similar to the description of the efficiency at the input IDT, represented as C_2F_k. The total output microwave voltage is obtained by the integration over all the SAW wave vectors, $V_{\rm out} = (C_2/2\pi)\int F_kq_ke^{ikL}dk$, where L is the distance between the input and output IDTs. Thus, the transmission parameters S_{12} and S_{21}, which are defined as ratios of the output voltage to the input one for two opposite directions of the signal propagation (from the port "1" to the port "2" and vice versa) are equal to:

$$S_{12,21} = \frac{C_1C_2}{2\pi i}\int \frac{\omega - (\omega_{\rm SW} - i\Gamma_{\rm SW})}{(\omega - \omega_1)(\omega - \omega_2)}F_k^2e^{\pm ikL}dk\,, \quad (20)$$

where S_{12} differs from S_{21} by the sign in front of the length L of the SAW line, and both IDTs are assumed to be the same. In a general case this expression cannot be further simplified, because the widths of the magneto-elastic bandgaps, the SW damping rate and the characteristic width of the function F_k can be of the same order of magnitude. In the limiting case of the absence of magneto-elastic coupling and a sufficiently wide spectrum of the IDT (i.e. in the case when the range of variation of the function F_k is much larger than $\Gamma_{\rm SAW}/c_{\rm SAW}$) Eq. (20) simplifies to the form: $S_{12,21} = (C_1C_2/c_{\rm SAW})\exp[-\Gamma_{\rm SAW}L/c_{\rm SAW}]$. The calculation of the coefficients C_1, C_2 requires an accurate accounting of the piezoelectric coupling and impedance matching between the SAW line and the external circuit, and lies beyond the scope of this article. Below, we use the normalization $C_1C_2/c_{\rm SAW} = 1$, i.e. we consider only the effects of the propagation losses of magneto-elastic waves and the spatial spectra of IDTs, given by F_k.

As it was pointed above, the widths of the magneto-elastic badgaps $\Delta\omega = 2|\kappa_k|$ are several orders of magnitude larger than the SAW linewidth, $\Gamma_{\rm SAW} \ll \Delta\omega$, and, at the same time the SW linewidth is, typically, larger than the width of the magneto-acoustic bandgap $\Gamma_{\rm SW} > \Delta\omega$. An example of the transmission characteristics calculated for this case is given in Fig. 4. For these calculation we used the thickness of a polycrystalline Ni layer of $t_{\rm Ni} = 5\,$nm, which is smaller than optimum thickness, in order to demonstrate, that a significant nonreciprocity of the transmission characteristic

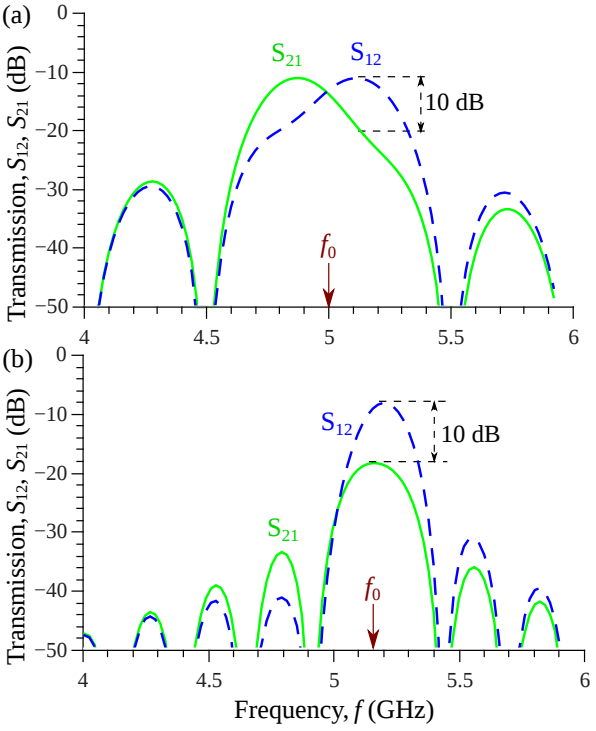

FIG. 4. Transmission characteristics of the SAW lines with a polycrystalline Ni film ($\alpha_G = 0.045$) having different IDTs for two opposite directions of the wave propagation (S_{12} (dashed line) and S_{21} (solid line)): (a) – IDT1 with central frequency $f_0 = 5\,\mathrm{GHz}$, number of fingers $N_f = 10$, and (b) – IDT2 with $f_0 = 5.16\,\mathrm{GHz}$, $N_f = 20$. The thickness of the Ni layer was $t_{\mathrm{Ni}} = 5\,\mathrm{nm}$, SAW line length $L = 250\,\mu\mathrm{m}$, bias magnetic field $B_e = 82\,\mathrm{mT}$ was applied at the angle $\phi = \pi/4$ to the line axis.

can be achieved not only in the unique optimum case. We have chosen the central frequency of the badgaps of 5 GHz, and the Gilbert damping parameter of the Nickel layer was chosen to be $\alpha_G = 0.045$, which is a typical value for polycrystalline Ni films [51]. For these parameters the spectral widths are: $\Gamma_{\mathrm{SAW}}/(2\pi) = 500\,\mathrm{kHz}$, $\Gamma_{\mathrm{SW}}/(2\pi) = 360\,\mathrm{MHz}$ and $\Delta\omega = 2|\kappa_k|/(2\pi) = 60\,\mathrm{MHz}$.

The parameters of the SAW line transmission characteristics can be adjusted by the selection of the IDT central frequency f_0 and the number of IDT fingers. For example, if the IDT central frequency f_0 lies between the magneto-elastic bandgaps and the spectrum of the IDT is wide enough to cover both bandgaps (small number of fingers), then the transmission characteristic contains two nonreciprocal bands where the transmission reaches a maximum value at different frequencies for the opposite wave propagation directions (see Fig. 4(a)). In contrast, if f_0 lies within one of the bandgaps and the IDT spectrum is narrow (large number of fingers), there is one main unidirectional transmission band, as shown in Fig. 4(b). The isolation in both of cases is close to 10 dB, while the propagation losses at the transmission maximum do not exceed 10 dB. We note, that these values of the isolation are much larger than the ones that were observed for a single Ni film on a $LiNbO_3$ substrate (without Pt) [32], and can be easily measured and, possibly, used in applications.

The isolation of the SAW line with magneto-elastic coupling can be substantially improved if a high-quality ferromagnetic film is used. As one can show form Eq. (19), the damping of the magneto-elastic waves at the crossing point depends on the relative values of the magneto-elastic coupling coefficient $|\kappa_k|$ and the SW linewidth Γ_{SW}. If $|\kappa_k| > (\Gamma_{\mathrm{SW}} + \Gamma_{\mathrm{SAW}})/2$, the damping rate of the hybridized waves is $\Gamma_{1,2} = (\Gamma_{\mathrm{SW}} - \Gamma_{\mathrm{SAW}})/2$. Otherwise, for $|\kappa_k| < (\Gamma_{\mathrm{SW}} + \Gamma_{\mathrm{SAW}})/2$, the damping rate of the magneto-acoustic waves is equal to $\Gamma_{1,2} = (\Gamma_{\mathrm{SW}} + \Gamma_{\mathrm{SAW}})/2 \pm \sqrt{(\Gamma_{\mathrm{SW}} - \Gamma_{\mathrm{SAW}})^2/4 - |\kappa_k|^2}$, i.e. the damping rate of one of the hybridized magneto-acoustic waves decreases with the increase of Γ_{SW}, and, in the limit $\Gamma_{\mathrm{SW}} \gg |\kappa_k|$, it is reduced to $\Gamma_1 \to \Gamma_{\mathrm{SAW}}$. Naturally, this low-damping hybridized wave makes a dominant contribution to the signal transmission rate, and the isolation in the transmission line decreases in spite of the fact that the signal frequency lies within a magneto-acoustic bandgap.

Thus, to maximize the influence of the magneto-elastic coupling on the signal transmission, the SW damping rate should be $\Gamma_{\mathrm{SW}} < 2|\kappa_k|$, while the use of ferromagnetic materials with high magnetic damping leaves SAW transmission almost unaffected.

For the studied heterostructure $LiNbO_3$/Ni/Pt such an optimum case could be realized if high-quality monocrystalline Ni film is used. In our numerical example illustrated in Fig. 5 we used a high quality Ni film with Gilbert damping constant of $\alpha_G = 0.014$ [56]. Here we have chosen the Ni layer thickness of $t_{\mathrm{Ni}} = 9\,\mathrm{nm}$, for which $2\kappa_k/(2\pi) = 105\,\mathrm{MHz}$ and $\Gamma_{\mathrm{SW}} = 104\,\mathrm{MHz}$. As it is clear from Fig. 5, the isolation in this case is increased remarkably, up to 45 dB and, also, this isolation exists in a rather wide frequency band.

It follows from Eq. (20), that the maximum achievable isolation in such a SAW transmission line is of the order of $S_{12} - S_{21} \sim \exp[(\Gamma_{\min} - \Gamma_{\mathrm{SAW}})L/c_{\mathrm{SAW}}]$, where $\Gamma_{\min} = \min \mathrm{Im}[\omega_{1,2}]$ is the smallest damping rate of the hybridized magneto-elastic waves. This maximum isolation is achieved at the frequency in the center of one of the magneto-elastic bandgaps, provided the excitation spectra of the used IDT is sufficiently narrow, compared to the bandgap width. This can be achieved using an IDT with a sufficiently large number of "fingers" N_f.

As it was pointed out previously, if the magneto-elastic coupling is relatively weak $|\kappa_k| < (\Gamma_{\mathrm{SW}} + \Gamma_{\mathrm{SAW}})/2$, we get $\Gamma_{\min} = (\Gamma_{\mathrm{SW}} + \Gamma_{\mathrm{SAW}})/2 - \sqrt{(\Gamma_{\mathrm{SW}} - \Gamma_{\mathrm{SAW}})^2/4 - |\kappa_k|^2}$. In this case a weak damping of one of the hybridized magneto-elastic waves strongly limits the maximum achievable isolation, and an increase of on the number N_f of the IDT fingers does not lead to a significant improvement of the isolation. For example, for the parameters used in Fig. 4(b) the increase of N_f from $N_f = 20$ to $N_f = 100$ gives only 1 dB of the isolation enhancement.

In contrast, in the optimum case of a strong cou-

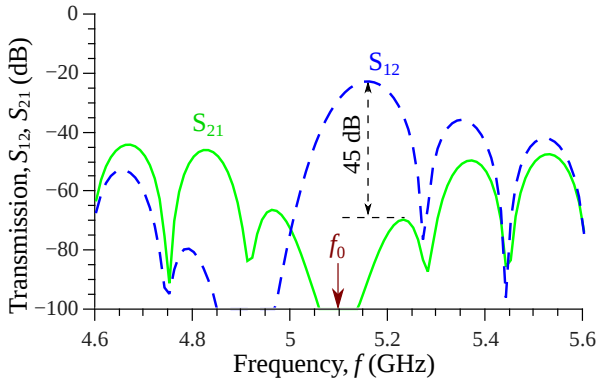

FIG. 5. Transmission characteristics of a SAW line with a monocrystalline Ni film ($\alpha_G = 0.014$) for two opposite directions of the wave propagation (S_{12} (dashed line) and S_{21} (solid line)). The thickness of the Ni layer was $t_{\rm Ni} = 9$ nm, SAW line length $L = 250\,\mu$m, IDT central frequency $f_0 = 5.095$ GHz, number of fingers $N_f = 30$, bias magnetic field $B_e = 45$ mT was applied at the angle $\phi = \pi/4$ to the line axis.

pling and a high-quality FM layer, when $|\kappa_k| > (\Gamma_{\rm SW} + \Gamma_{\rm SAW})/2$, the maximum isolation could be very high, so the signal level in one direction can be below the level of a thermal noise. For example, it follows from Fig. 5, that at the frequency 5.09 GHz the isolation is 84 dB, and can be made even higher for the increased number N_f of IDT "fingers". This, however, will lead to a severe limitation in the frequency band of the transmitted signal.

Thus, we have shown that by using a well-known acoustic and magnetic materials, such as $LiNbO_3$ in combination with a Ni film covered by a thin layer of Pt, it is possible to achieve the transmission of hybridized magneto-acoustic waves with quite a large level of nonreciprocal isolation. The characteristics of such a nonreciprocal magneto-acoustic isolator could be further improved using ferromagnetic materials with lower damping. A promising materials for this purpose could be CoFe alloys, which, at a certain composition, show ultralow magnetic damping of $\alpha_G = 0.0014$ [57]. Unfortunately, the magneto-elastic properties and the DMI of these alloys have not been studied yet.

IV. CONCLUSION

In this work we presented a general theory of a linear magneto-elastic coupling between the spin and acoustic waves propagating in an arbitrary magnetic / nonmagnetic layered structure and having arbitrary mode profiles. The developed theory uses the relative weakness of the magneto-elastic interaction, and reduces the problem to a standard form of equations for coupled oscillators. The theory provides a simple method for the calculation of the magneto-elastic wave dispersion, damping parameters of the coupled waves, as well as for the determination of the condition of nonzero magneto-elastic interaction between the acoustic and spin waves.

Using the developed theory we demonstrated that the SW nonreciprocity, induced by the IDMI, can be "transferred" to the "hybridized SAWs" existing in piezoelectric / ferromagnetic / heavy metal heterostructures. The magneto-elastic interaction results in the appearance of bandgaps in the spectra of magneto-elastic surface waves, and, because of the IDMI-induced SW nonreciprocity, these bandgaps exist at different frequency and wave number positions for the opposite wave propagation directions. The widths of these bandgaps and the frequency separation between them can be optimized by a proper selection of the in-plane magnetization angle ($\phi \approx \pi/4$ relative to the direction of the SAW propagation) and the thickness of a ferromagnetic layer (about 8-9 nm for the studied $LiNbO_3$/Ni/Pt heterostructure), while the central frequency of the bandgaps can be tuned by varying the magnitude of the bias magnetic field.

We demonstrated, that the transmission characteristics of the surface magneto-elastic waves can be substantially nonreciprocal, while having relatively low direct insertion losses. Our calculations show that for $LiNbO_3$ covered by a think Ni/Pt layer it is possible to achieve the isolation of 10-45 dB, while maintaining the SAW propagation losses below 10-20 dB. The isolation could be further improved by a selection of a proper ferromagnetic material having large values of the magnetostriction and IDMI, but low magnetic losses.

ACKNOWLEDGEMENTS

This work was supported in part by the grant from the Center for NanoFerroic Devices (CNFD) and Nanoelectronics Research Initiative (NRI), by the grants Nos. EFMA-1641989 and ECCS-1708982 from the NSF of the USA, and by the DARPA M3IC grant under the contract W911-17-C-0031. RV acknowledges support from the Ministry of Education and Science of Ukraine, project 0118U004007. IL acknowledges support from DARPA SPAR (grant No HR0011-17-2-2005) and the Russian Science Foundation (project No 14-19-00760).

[1] C. Campbell, *Surface Acoustic Wave Devices and Their Signal Processing Applications* (Academic Press, 1989).
[2] B. A. Auld, *Acoustic Fields and Waves in Solids* (Krieger Pub Co, 1990).
[3] D. Morgan, *Surface Acoustic Wave Filters: With Applications to Electronic Communications and Signal Processing (Studies in Electrical and Electronic Engineering)*, 2nd ed. (Academic Press, London, 2010).

[4] E.A. Ash, A.A. Oliner, G.W. Farnell, H.M. Gerard, A.A. Oliner, A.J. Slobodnik, and H.I. Smith, *Acoustic Surface Waves*, edited by A.A. Oliner, Topics in Applied Physics (Springer Berlin Heidelberg, 2014).

[5] A. G. Gurevich and G. A. Melkov, *Magnetization Oscillations and Waves* (CRC Press, New York, 1996).

[6] B. K. Kuanr, V. Veerakumar, R. Marson, S. R. Mishra, R. E. Camley, and Z. Celinski, "Nonreciprocal microwave devices based on magnetic nanowires," Appl. Phys. Lett. **94**, 202505 (2009).

[7] J. Heil, B. Lüthi, and P. Thalmeier, "Nonreciprocal surface-acoustic-wave propagation in aluminum," Phys. Rev. B **25**, 6515 (1982).

[8] R. Fleury, D. L. Sounas, C. F. Sieck, M. R. Haberman, and A. Alù, "Sound Isolation and Giant Linear Nonreciprocity in a Compact Acoustic Circulator," Science **343**, 516 (2014).

[9] B. Liang, B. Yuan, and J.-C. Cheng, "Acoustic Diode: Rectification of Acoustic Energy Flux in One-Dimensional Systems," Phys. Rev. Lett. **103**, 104301 (2009).

[10] B. Liang, X. S. Guo, J. Tu, D. Zhang, and J. C. Cheng, "An acoustic rectifier," Nat. Mater. **9**, 989 (2010).

[11] N. Boechler, G. Theocharis, and C. Daraio, "Bifurcation-based acoustic switching and rectification," Nat. Mater. **10**, 665 (2011).

[12] Z.-M. Gu, J. Hu, B. Liang, X.-Y. Zou, and J.-C. Cheng, "Broadband non-reciprocal transmission of sound with invariant frequency," Sci. Rep. **6**, 19824 (2016).

[13] J. R. Eshbach and R. W. Damon, "Surface Magnetostatic Modes and Surface Spin Waves," Phys. Rev. **118**, 1208 (1960).

[14] G. A. Melkov, V. I. Vasyuchka, V. V. Lazovskiy, V. S. Tiberkevich, and A. N. Slavin, "Wave front reversal with frequency conversion in a nonreciprocal medium," Appl. Phys. Lett. **89**, 252510 (2006).

[15] M. Mruczkiewicz, M. Krawczyk, G. Gubbiotti, S. Tacchi, Yu. A. Filimonov, D. V. Kalyabin, I. V. Lisenkov, and S. A. Nikitov, "Nonreciprocity of spin waves in metallized magnonic crystal," New J. Phys. **15**, 113023 (2013).

[16] R. Verba, V. Tiberkevich, E. Bankowski, T. Meitzler, G. Melkov, and A. Slavin, "Conditions for the spin wave nonreciprocity in an array of dipolarly coupled magnetic nanopillars," Appl. Phys. Lett. **103**, 082407 (2013).

[17] I. Lisenkov, V. Tyberkevych, A. Slavin, P. Bondarenko, B. A. Ivanov, E. Bankowski, T. Meitzler, and S. Nikitov, "Spin-wave edge modes in finite arrays of dipolarly coupled magnetic nanopillars," Phys. Rev. B **90**, 104417 (2014).

[18] R. Verba, E. Bankowski, T. Meitzler, V. Tiberkevich, and A. Slavin, "Nonreciprocal Spin Waves in a Magnonic Crystal with In-Plane Static Magnetization," SPIN **06**, 1640013 (2016).

[19] R. L. Melcher, "Linear Contribution to Spatial Dispersion in the Spin-Wave Spectrum of Ferromagnets," Phys. Rev. Lett. **30**, 125 (1973).

[20] D. Cortés-Ortuño and P. Landeros, "Influence of the Dzyaloshinskii–Moriya interaction on the spin-wave spectra of thin films," J. Phys.: Cond. Matter **25**, 156001 (2013).

[21] J.-H. Moon, S.-M. Seo, K.-J. Lee, K.-W. Kim, J. Ryu, H.-W. Lee, R. D. McMichael, and M. D. Stiles, "Spin-wave propagation in the presence of interfacial Dzyaloshinskii-Moriya interaction," Phys. Rev. B **88**, 184404 (2013).

[22] V. L. Zhang, K. Di, H. S. Lim, S. C. Ng, M. H. Kuok, J. Yu, J. Yoon, X. Qiu, and H. Yang, "In-plane angular dependence of the spin-wave nonreciprocity of an ultrathin film with Dzyaloshinskii-Moriya interaction," Appl. Phys. Lett. **107**, 022402 (2015).

[23] M. Tsutsumi, T. Bhattacharyya, and N. Kumagai, "Piezoelectricmagnetoelastic surface wave guided by interface between semiinfinite piezoelectric and magnetoelastic media," J. Appl. Phys. **46**, 5072 (1975).

[24] G. Komoriya and G. Thomas, "Magnetoelasticsurface waves on YIG substrate," J. Appl. Phys. **50**, 6459 (1979).

[25] Y. Shimizu, K. Hasegawas, and T. Yamada, "Nonreciprocity of saw velocity on a magnetized ferrite substrate," Electron. Comm. Japan. Pt. I, **63**, 1 (1980).

[26] C. Kittel, "Interaction of Spin Waves and Ultrasonic Waves in Ferromagnetic Crystals," Phys. Rev. **110**, 836 (1958).

[27] K. B. Vlasov, "Equations of motion for magnetization in deformed anisotropic media," Sov. Phys. JETP **16**, 1505 (1963).

[28] R. L. Comstock, "Parallel Pumping of Magnetoelastic Waves in Ferromagnets," J. Appl. Phys. **35**, 2427 (1964).

[29] M. Weiler, L. Dreher, C. Heeg, H. Huebl, R. Gross, M. S. Brandt, and S. T. B. Goennenwein, "Elastically Driven Ferromagnetic Resonance in Nickel Thin Films," Phys. Rev. Lett. **106**, 117601 (2011).

[30] P. G. Gowtham, T. Moriyama, D. C. Ralph, and R. A. Buhrman, "Traveling surface spin-wave resonance spectroscopy using surface acoustic waves," J. Appl. Phys. **118**, 233910 (2015).

[31] V. Polewczyk, K. Dumesnil, D. Lacour, M. Moutaouekkil, H. Mjahed, N. Tiercelin, S. Petit Watelot, H. Mishra, Y. Dusch, S. Hage-Ali, O. Elmazria, F. Montaigne, A. Talbi, O. Bou Matar, and M. Hehn, "Unipolar and Bipolar High-Magnetic-Field Sensors Based on Surface Acoustic Wave Resonators," Phys. Rev. Applied **8**, 024001 (2017).

[32] R. Sasaki, Y. Nii, Y. Iguchi, and Y. Onose, "Nonreciprocal propagation of surface acoustic wave in Ni/$LiNbO_3$," Phys. Rev. B **95**, 020407 (2017).

[33] P. G. Gowtham, T. Moriyama, D. C. Ralph, and R. A. Buhrman, "Traveling surface spin-wave resonance spectroscopy using surface acoustic waves," Journal of Applied Physics **118**, 233910 (2015).

[34] X. Li, D. Labanowski, S. Salahuddin, and C. S. Lynch, "Spin wave generation by surface acoustic waves," J. Appl. Phys. **122**, 043904 (2017).

[35] R. Duflou, F. Ciubotaru, A. Vaysset, M. Heyns, B. Sorée, I. P. Radu, and C. Adelmann, "Micromagnetic simulations of magnetoelastic spin wave excitation in scaled magnetic waveguides," Appl. Phys. Lett. **111**, 192411 (2017).

[36] A. Barra, A. Mal, G. Carman, and A. Sepulveda, "Voltage induced mechanical/spin wave propagation over long distances," Appl. Phys. Lett. **110**, 072401 (2017).

[37] V. V. Naletov, G. de Loubens, G. Albuquerque, S. Borlenghi, V. Cros, G. Faini, J. Grollier, H. Hurdequint, N. Locatelli, B. Pigeau, A. N. Slavin, V. S. Tiberkevich, C. Ulysse, T. Valet, and O. Klein, "Identification and selection rules of the spin-wave eigenmodes in a normally magnetized nanopillar," Phys. Rev. B **84**, 224423 (2011).

[38] R. Verba, G. Melkov, V. Tiberkevich, and A. Slavin, "Collective spin-wave excitations in a two-dimensional array of coupled magnetic nanodots," Phys. Rev. B **85**,

014427 (2012).
[39] O. Dzyapko, I. Lisenkov, P. Nowik-Boltyk, V. E. Demidov, S. O. Demokritov, B. Koene, A. Kirilyuk, T. Rasing, V. Tiberkevich, and A. Slavin, "Magnon-magnon interactions in a room-temperature magnonic Bose-Einstein condensate," Phys. Rev. B **96**, 064438 (2017).
[40] S. Chikazumi, *Physics of Ferromagnetism (International Series of Monographs on Physics)* (Oxford University Press, 2009).
[41] Comparing to Refs. 37–39 here we add the dimensional multiplier M_s/γ, which aligns the units of the spin-wave norm the same units as acoustic normalization constant.
[42] D. Kalyabin, I. Lisenkov, Y.P. Lee, and S. Nikitov, "Frequency separation of surface acoustic waves in layered structures with acoustic metamaterials," Phot. Nano. Fund. Appl. **12**, 239 (2014).
[43] T. Brächer, O. Boulle, G. Gaudin, and P. Pirro, "Creation of unidirectional spin-wave emitters by utilizing interfacial Dzyaloshinskii-Moriya interaction," Phys. Rev. B **95**, 064429 (2017).
[44] M. Kostylev, "Interface boundary conditions for dynamic magnetization and spin wave dynamics in a ferromagnetic layer with the interface Dzyaloshinskii-Moriya interaction," J. Appl. Phys. **115**, 233902 (2014).
[45] A. A. Oliner, ed., *Acoustic Surface Waves* (Springer, NY, 1978).
[46] Pawe Sobieszczyk, Mirosaw Gazka, Dominik Trzupek, and Piotr Zieliski, "Propagation of surface waves and surface resonances along cylindrical cavities in materials with any allowed poissons ratio - part i: Clean inner surface," physica status solidi (b) **252**, 15951604 (2015).
[47] S. Tacchi, R. E. Troncoso, M. Ahlberg, G. Gubbiotti, M. Madami, J. Åkerman, and P. Landeros, "Interfacial Dzyaloshinskii-Moriya Interaction in Pt/CoFeB Films: Effect of the Heavy-Metal Thickness," Phys. Rev. Lett. **118**, 147201 (2017).
[48] L. D. Landau, L. P. Pitaevskii, A. M. Kosevich, and E. M. Lifshitz, *Theory of Elasticity: Volume 7 (Course of Theoretical Physics)* (Butterworth-Heinemann, 2012).
[49] X. Chen, M. Mohammad, J. Conway, B. Liu, Y. Yang, and T.-L. Ren, "High performance lithium niobate surface acoustic wave transducers in the 4–12 GHz super high frequency range," J. Vac. Sci. Technol. B Nanotechnol. Microelectron. **33**, 06F401 (2015).
[50] A. S. Andrushchak, B. G. Mytsyk, H. P. Laba, O. V. Yurkevych, I. M. Solskii, A. V. Kityk, and B. Sahraoui, "Complete sets of elastic constants and photoelastic coefficients of pure and MgO-doped lithium niobate crystals at room temperature," J. Appl. Phys. **106**, 073510 (2009).
[51] J. Walowski, M. Djordjevic Kaufmann, B. Lenk, C. Hamann, J. McCord, and M. Münzenberg, "Intrinsic and non-local Gilbert damping in polycrystalline nickel studied by Ti : sapphire laser fs spectroscopy," J. Phys. D: Appl. Phys. **41**, 164016 (2008).
[52] D. Sander, "The correlation between mechanical stress and magnetic anisotropy in ultrathin films," Rep. Progr. Phys. **62**, 809 (1999).
[53] G. Chen, T. Ma, A. T. N'Diaye, H. Kwon, C. Won, Y. Wu, and A. Schmid, "Tailoring the chirality of magnetic domain walls by interface engineering," Nat. Comm. **4**, 2671 (2013).
[54] W. S. Wilson and G. M. Atkinson, "A Comparison of Surface Acoustic Wave Modeling Methods," in *Nanotechnology 2009: Biofuels, Renewable Energy, Coatings, Fluidics and Compact Modeling*, Vol. 3 (NSTI, 2009) p. 347.
[55] K. Yamanouchi, "Generation, propagation, and attenuation of 10 GHz-range SAW in $LiNbO_3$," in *1998 IEEE Ultrasonics Symposium. Proceedings (Cat. No. 98CH36102)*, Vol. 1 (1998) pp. 57–62 vol.1.
[56] N. Inaba, H. Asanuma, S. Igarashi, S. Mori, F. Kirino, K. Koike, and H. Morita, "Damping Constants of Ni-Fe and Ni-Co Alloy Thin Films," IEEE Trans. Magn. **42**, 2372 (2006).
[57] A. J. Lee, J. T. Brangham, Y. Cheng, S. P. White, W. T. Ruane, B. D. Esser, D. W. McComb, P. C. Hammel, and F. Yang, "Metallic ferromagnetic films with magnetic damping under 1.4×10^{-3}," Nat. Comm. **8**, 234 (2017).